KRONOS FUSION ENERGY

PAPER 2.101 · THE KRONOS 2026 SERIES

# *Red-Teaming the Frozen Design Point: Current-Drive and beta-Headroom Margins for a Spherical-Tokamak Breeder and Thermal-Barrier versus Centrifugal Plug Alternatives for the Mirror Burner*

A design that publishes its negatives is honest; a design that then bounds whether each negative can be closed is useful. We formalise and execute an adversarial red-team of the...

Read it live — 3-D model · physics validator · film series

BY P I FORD

2026 · EDITORIAL EDITION

THE OFFICIAL RECORD

# What this document is, and how to read its numbers

This is a combined editorial. It gathers, in one volume, the two design studies Kronos Fusion Energy released in 2026 — a compact spherical-tokamak tritium/helium-3 breeder and a deuterium–helium-3 tandem-mirror generator — together with the intellectual-property estate, the people, and, in the internal edition, the full commercial case. The scientific text is the same text that appears in the arXiv preprints and the journal submissions; the editorial adds the apparatus a reader needs to hold the whole program at once, and nothing in the physics is altered to fit it.

## THE HONESTY STANCE IS THE ASSET

Every headline quantity carries an **evidence class** — DERIVED RECOMPUTED MEASURED REQUIREMENT — and, where a number is a modelled extrapolation rather than a demonstrated value, it is labelled as such and its downside is shown next to it. Several quantities in the underlying corpus moved after first publication; where a value has been withdrawn or restated, the record says so plainly. This is deliberate: a diligence team will find the load-bearing assumptions, so the document surfaces them first.

## TWO EDITIONS

This volume is issued in two editions. The **public edition** (light) carries the physics and the design only — no dollar, price, or per-kilogram figure appears anywhere in it. The **internal edition** (dark) adds the economics, the funding architecture, and the defense-commercial analysis, and is marked *Confidential* accordingly; it is not for public distribution. Where the commercial case rests on a modelled assumption rather than a demonstrated one, it is labelled as such and its downside is shown alongside it, on the same terms as the physics.

| | |
|---|---|
| TITLE | The Kronos Fleet — Hyperion · Aegis · MetroVolt: A Combined Design & Commercialization Study |
| AUTHOR | Priyanca Ford, Founder & CEO, on behalf of Kronos Fusion Energy |
| EDITION | 2026 Combined Editorial · first issue |
| COMPANION WORKS | The five-paper arXiv drop — (1) Breeder, (2) Burner, (3) REBCO magnet & tape, (4) Direct Energy Conversion, (5) AI/ML/Quantum control — with matching numbered Zenodo deposits, plus the IOP journal and IAEA-FEC submissions. Patents were filed before the drop. |
| NAMING | Hyperion = the breeder; Aegis (defense) and MetroVolt (data-center) = one generator in two housings. Internal mode letters (D1, L) do not appear on public surfaces. |
| STATUS | Conceptual design & simulation study. Nothing herein is a construction commitment. |

HOW TO READ THIS VOLUME

# The fleet at a glance, and the way its numbers are marked

This volume opens with *Orientation*, presents the five research papers as a bound sequence, and closes with the *Apparatus*. *Foundations* sets out the three general results both machines rest on. *Paper One* is the Hyperion breeder; *Paper Two* the Aegis / MetroVolt generator; *Papers Three, Four and Five* are the enabling science — high-field REBCO magnets and tape, direct energy conversion, and the AI / ML / quantum control stack. A *Digital Twin & 3-D Model* part follows, then the *Environmental* profile. The *Economics* and levelized cost and the *Business Case* and diligence record appear in the internal edition only; the *Simulations* proof record and the Apparatus — patent portfolio, team, limitations, and sources — close both editions.

## THE FLEET AT A GLANCE

| | HYPERION | AEGIS | METROVOLT |
|---|---|---|---|
| **Role** | Strategic-isotope foundry | Defense installation power | Campus power |
| **Machine** | **Spherical tokamak** | **Tandem mirror** | **Tandem mirror** |
| **Fuel** | Deuterium–tritium | Deuterium–helium-3 | Deuterium–helium-3 |
| **Delivers** | Tritium · $^{3}$He · 14 MeV n | Resilient installation power | Firm campus power |
| **Physics bar** | **Fusion gain only** | Closure (gates named) | Closure + lunar $^{3}$He |
| **In the fleet** | Breeds the fuel | Proves the generator | Commercial destination |

## HOW THE NUMBERS ARE MARKED

Every headline quantity carries an evidence class — DERIVED from first principles, RECOMPUTED from raw data, MEASURED in hardware, or a REQUIREMENT yet to be met. Financial figures carry a case label and are confined to the internal (confidential) edition. Values that moved after first publication are shown as withdrawn or restated rather than quietly changed. A capability you can evaluate is one whose limits are on the page.

ABSTRACT

# Red-Teaming the Frozen Design Point: Current-Drive and beta-Headroom Margins for a Spherical-Tokamak Breeder and Thermal-Barrier versus Centrifugal Plug Alternatives for the Mirror Burner

A design that publishes its negatives is honest; a design that then bounds whether each negative can be closed is useful. We formalise and execute an adversarial red-team of the binding engineering gates of a compact, negative-triangularity spherical-tokamak breeder ($Q = 3.076$, $P_{\text{fus}} = 85.04\,MW$, $I_p = 9.66\,MA$, $\delta = -0.30$, $B_0 = 8\,T$, $\kappa = 2.0$, $R_0 = 1.20\,m$, aspect ratio $A = 2.5$, centrepost peak field $16.84\,T$) and its separate deuterium–helium-3 tandem-mirror burner ($Q_E = 1.318$, neutron fraction $f_n = 5.44\%$, plug field $26.49\,T$, direct-conversion efficiency $\eta_{\text{DEC}} = 0.49$). The method is stated as a min–max feasibility program: with the mission anchors held fixed we seek the design move that maximises the weakest normalised gate margin, and we bound each candidate with a conservative reduced-order screening model whose pass implies a high-fidelity pass. Four gates bind. The breeder current-drive burden, which exceeds fusion power in the solenoid-free baseline ($P_{\text{CD}} = 118.5\,MW$ against $P_{\text{fus}} = 85.04\,MW$), falls to $50\,MW$ ($-58\%$, below fusion power) at an advanced operating point that lifts the bootstrap fraction from $f_{\text{bs}} = 0.155$ into unused Troyon headroom while raising the $14\,MeV$ source by $1.68\times$; tritium closure, fragile against the beryllium-multiplier fraction, is restored to a multiplier-independent sub-additive upper bound of $\text{TBR} \leq 1.204$ above the $1.05$ self-sufficiency threshold; and a reduced-standoff re-entrant materials-test port reaches [redacted] without changing mission power. For the burner, the entry gate — the plug-to-central density ratio $n_p/n_c = 16$ set by the Boltzmann relation $n_p/n_c = \exp(e\phi_i/T_e)$ — is attacked two ways: a hot-electron thermal barrier acting inside the exponent lowers the required ratio to $\approx 3.5$, and a centrifugal rotating-mirror architecture replaces the electrostatic plug with a centrifugal potential and removes the density-ratio gate entirely ($\approx 1.0$), at the cost of a new, unresolved rotational (interchange) stability question. Every headline is a reduced-order screening bound produced by, and cross-checked against, the NVIDIA GPU HPC campaign (nonlinear CGYRO, OpenMC/DAGMC, WarpX, and a mirror kinetic solver); its value is to tell high-fidelity computation where to spend its time, and to show that the closing levers were hiding in unused design headroom rather than requiring new physics.

Open-access deposit (code & data, CC BY 4.0): DOI 10.5281/zenodo.22645720 · Zenodo community *kronos_fusion_energy*. Explore it live: interactive 3-D model · physics validator.

**Keywords:** fusion design · current drive · bootstrap fraction · Troyon limit · tritium breeding ratio · plug density · tandem mirror · thermal barrier · centrifugal mirror · reduced-order screening

CONTENTS

# Table of Contents

NOMENCLATURE

# Symbols, units, and the names of things

| | |
|---|---|
| $Q$ | plasma (fusion) gain, $P_{fus}/P_{aux}$ |
| $Q_E$ | engineering gain, net electric out / recirculating in |
| $H_{98}$ | confinement enhancement over the IPB98(y,2) scaling |
| $Z_{eff}$ | effective ion charge |
| $c_{ee}$ | electron–electron bremsstrahlung leading coefficient, 2.120022 (exact) |
| $\tau_E$ | energy confinement time |
| $I_p$ | plasma current |
| $R_0, a$ | major radius, minor radius |
| $\kappa, \delta$ | elongation, triangularity |
| $\beta_N$ | normalized plasma beta (Troyon-normalized) |
| *TBR* | tritium breeding ratio |
| *DEC* | direct energy conversion |
| *CF* | plant capacity factor (availability) |
| *FOAK / NOAK / BOAK* | first / n$^{th}$ / best of a kind |
| *Hyperion* | the ST breeder (internal: Mode D2) |
| *Aegis* | the generator, defense/installation housing (internal: Mode M) |
| *MetroVolt* | the generator, data-center housing (Mode M) |

§ 1

# Introduction

## HONEST NEGATIVES AND THE VALUE OF BOUNDING THEM

A design program earns trust by stating its negatives plainly. But a stated negative is only the beginning of the engineering question: is it a hard physical limit, or a bounded, closable gap for which a named path exists? The two demand very different follow-on work — one is a reason to stop, the other a direction for the next high-fidelity calculation. This paper treats the binding gates of the two Kronos machines as *adversarial* targets. For each honest negative we brainstorm a small set of alternatives, bound each with a conservative reduced-order or analytic model, rank them, and promote only the winners to high-fidelity validation; ruled-out alternatives are reported as negatives rather than hidden. The output is deliberately modest in kind: a set of *screening bounds* that state the direction and magnitude of each closing lever, explicitly not banked results.

## THE TWO MACHINES AND THEIR FROZEN ANCHORS

The Kronos breeder (Hyperion) is a compact spherical tokamak (ST) that holds a large plasma current in a small volume, which is exactly what makes it an attractive $14\,MeV$ neutron source and strategic-materials platform [1,2,3] and, at the same time, what makes it demanding to sustain and to protect. Its frozen design point is $I_p = 9.66\,MA$ at a major radius of only $R_0 = 1.20\,m$ ($A = 2.5$) behind a centrepost magnet at a peak field of $16.84\,T$, in a negative-triangularity ($\delta = -0.30$), high-elongation ($\kappa = 2.0$) regime that accesses good confinement without an edge pedestal and its edge-localised-mode cycle [4,5]. The corresponding gain and power are $Q = 3.076$ and $P_{\text{fus}} = 85.04\,MW$. The Kronos burner is a physically distinct machine: a deuterium–helium-3 (D–$^3$He) tandem mirror sized for low-neutron, sited operation ($Q_E = 1.318$, $f_n = 5.44\%$), whose ion-confining electrostatic plug is held by a separate, higher-field coil at $26.49\,T$, with charged-particle power recovered by direct energy conversion at $\eta_{\text{DEC}} = 0.49$. Throughout we keep the two magnets — the breeder centrepost at $16.84\,T$ and the burner plug at $26.49\,T$ — as the distinct devices they are, and never conflate their fields.

## PRIOR ART

The individual gates we attack are each mature subjects. Solenoid-free current sustainment in an ST rests on aligning a large bootstrap fraction with externally driven current [6,7]; the pressure available for that alignment is capped by the Troyon normalised-$\beta$ limit and the external-kink margin [8,9]. Tritium self-sufficiency in a compact device is a well-known knife-edge, with the required breeding margin set against inventory, recycling and blanket coverage [10,11]. Fusion materials qualification needs a high-fluence, prototypical-spectrum irradiation source, and the displacement-per-atom (dpa) figure is computed by the standard NRT/arc-dpa conventions [12,13]. On the burner side, the tandem-mirror ion-confining potential and its density-ratio requirement descend directly from Pastukhov′s ambipolar-loss theory [14,15] and the thermal-barrier concept that decouples the plug electron population [16,17,18]; the alternative of replacing the electrostatic plug by supersonic $E \times B$ rotation has its own experimental lineage in centrifugally confined and rotating mirrors [19,20,21,22]. What has not been done for these two specific machines is to treat all of these gates within a single adversarial framework that (i) states feasibility and the binding margin as a formal min–max, (ii) bounds each closing lever with a conservative reduced-order model whose pass is a sufficient condition for a high-fidelity pass, and (iii) ranks the alternatives and reports the losers.

## CONTRIBUTION

This paper contributes exactly that. We give (§2) the formal red-team program — the feasibility set, the binding margin, the epigraph min–max, and the screening-bound property that makes a cheap model admissible; the breeder current-drive/bootstrap/$\beta$-headroom balance, the tritium margin algebra, the materials-testing standoff geometry, and the burner plug-density gate with its thermal-barrier and centrifugal alternatives, all as explicit equations. We give (§3) the computational methodology: the reduced-order gate evaluator and its discretisation, the adversarial min–max solver and its convergence, and the high-fidelity anchors run on the NVIDIA GPU HPC campaign that verify the screening bounds. We give (§4) the results — the binding-margin map, the three breeder closures and the two burner alternatives — in eleven figures and four tables. We compare quantitatively to the published literature (§5), state the one honest gate the analysis does not resolve (§6), and conclude (§7). Every quantitative claim traces to a frozen result in the Kronos Physics De-Risking Register [28]; the serial identifiers (e.g. `BR-CX-07`) are given inline so each number is auditable, and the negative-triangularity confinement basis is now itself a de-risked result rather than an assumption [29,30].

§ 2

# Governing equations and the formal red-team problem

## FEASIBILITY, THE BINDING MARGIN, AND THE MIN–MAX

Let $\vec{p} \in \mathcal{P} \subset \mathbb{R}^d$ be the design vector and let each engineering requirement be written as a normalised gate function $g_k(\vec{p})$, $k = 1, \dots, K$, with the convention that $g_k(\vec{p}) \geq 0$ means "pass" and the numerical value is a margin. A design is feasible only in the intersection of the gate half-spaces,

$$\mathcal{F} = \bigcap_{k=1}^{K} \{\, \vec{p} : \; g_k(\vec{p}) \geq 0 \,\},$$

and the strength of a candidate point is its *worst* single gate,

$$m(\vec{p}) = \min_{1 \leq k \leq K} g_k(\vec{p}), \qquad k^*(\vec{p}) = \arg\min_k g_k(\vec{p}),$$

so a design is only as strong as its binding gate $k^*$. The frozen design point $\vec{p}_0$ has a binding gate and a (possibly negative) margin $m(\vec{p}_0)$; red-teaming is the adversarial dual of a feasibility search — rather than accept $m(\vec{p}_0)$, we ask for the admissible move that lifts the weakest gate the furthest while holding the mission anchors $\vec{a}(\vec{p}) = \vec{a}_0$ (here $Q$, $P_{\text{fus}}$, $I_p$, $\delta$, $B_0$, $\kappa$, $R_0$, $A$) fixed:

$$m^* = \max_{\vec{p} \in \mathcal{P}} \; \min_k g_k(\vec{p}) \quad \text{s.t.} \quad \vec{a}(\vec{p}) = \vec{a}_0.$$

Introducing the epigraph variable $t$ recasts (3) as the bottleneck program

$$\max_{\vec{p},\, t} \; t \quad \text{s.t.} \quad g_k(\vec{p}) \geq t \;\; \forall k, \qquad \vec{a}(\vec{p}) = \vec{a}_0, \qquad \vec{p} \in \mathcal{P}.$$

At any Karush–Kuhn–Tucker point of (4) the active gate constraints carry non-negative multipliers $\lambda_k$ that sum to unity, $\sum_{k \in \mathcal{A}} \lambda_k = 1$, and the stationarity condition $\sum_{k \in \mathcal{A}} \lambda_k \nabla g_k(\vec{p}^*) = \sum_j \mu_j \nabla a_j$ forces a *margin-equalisation* across the active set: at the optimum no single gate can be improved without degrading another that is equally binding. The red-team therefore does two things at once — it locates the binding gate $k^*$ (the honest failure surface, found rather than avoided) and it quantifies how far $m$ can be recovered under the mission constraints.

## THE SCREENING-BOUND PROPERTY

Solving (4) with high-fidelity $g_k$ is intractable inside a search. We instead evaluate a reduced-order surrogate $g_k^{\text{RO}}$ constructed to be *conservative*,

$$g_k^{\text{RO}}(\vec{p}) \;\leq\; g_k(\vec{p}) \qquad \forall \vec{p} \in \mathcal{P},$$

so that a pass under the surrogate is a sufficient condition for a pass under the true gate: $g_k^{\text{RO}}(\vec{p}) \geq 0 \Rightarrow g_k(\vec{p}) \geq 0$. Property (5) is what licenses a cheap model to make a rigorous, one-sided statement — a *screening bound*. Every headline number in this paper is such a bound: it states a guaranteed direction and a conservative magnitude, and its role is to point high-fidelity computation at the promising region of $\mathcal{P}$, not to bank a result.

## BREEDER GATE W1: CURRENT-DRIVE, BOOTSTRAP, AND $\beta$-HEADROOM

In the solenoid-free ST the flat-top toroidal current must be sustained non-inductively. The current balance is

$$I_p = I_{\text{bs}} + I_{\text{CD}} + I_{\text{seed}}, \qquad f_{\text{bs}} \equiv \frac{I_{\text{bs}}}{I_p},$$

so the externally driven fraction is $1 - f_{\text{bs}} - f_{\text{seed}}$ and the current-drive power follows from the dimensional current-drive figure of merit $\gamma_{\text{CD}} = n_{e20} R_0 I_{\text{CD}} / P_{\text{CD}}$ (units $10^{20}\ \text{A}\,\text{W}^{-1}\,\text{m}^{-2}$),

$$P_{\text{CD}} = \frac{n_{e20}\, R_0\, (1 - f_{\text{bs}} - f_{\text{seed}})\, I_p}{\gamma_{\text{CD}}}.$$

The bootstrap current is set, in the Sauter neoclassical closure, by the poloidal pressure through

$$f_{\rm bs} = c_{\rm bs}\sqrt{\epsilon}\,\beta_p, \qquad \epsilon = \frac{a}{R_0} = \frac{1}{A},$$

with $\beta_p$ the poloidal beta and $c_{\rm bs}$ an $O(1)$ coefficient fixed by the profile shape. The available pressure is bounded by the Troyon normalised limit and the no-wall external-kink margin,

$$\beta_N \equiv \frac{\beta_T\, a\, B_0}{I_p} \;\le\; \beta_N^{\rm crit} = g_T\,, \qquad \beta_T \propto \beta_p\left(\frac{B_p}{B_0}\right)^2,$$

so raising $\beta_p$ toward the ceiling raises $f_{\rm bs}$ by (8) and cuts $P_{\rm CD}$ by (7). The current-drive efficiency itself improves with electron temperature, $\gamma_{\rm CD} \propto T_e/n_e$ [7], so a hotter advanced point cuts $P_{\rm CD}$ a second way. Combining the two levers as a ratio removes the need to pin $\gamma_{\rm CD}$ absolutely:

$$\frac{P'_{\rm CD}}{P^0_{\rm CD}} = \underbrace{\frac{1-f'_{\rm bs}}{1-f^0_{\rm bs}}}_{\text{bootstrap}} \cdot \underbrace{\frac{\gamma^0_{\rm CD}}{\gamma'_{\rm CD}}}_{\text{efficiency}} \cdot \underbrace{\frac{n'_e}{n^0_e}}_{\text{density}}.$$

Finally, the neutron source scales as $S_n = \frac{1}{4} n_{\rm D} n_{\rm T} \langle\sigma v\rangle_{\rm DT} V$, so the same move to higher density and temperature raises the mission-relevant source. Equations (6)–(10) are the analytic content of W1: the lever is unused pressure headroom, not new physics.

## BREEDER GATE W2: TRITIUM-CLOSURE MARGIN ALGEBRA

Let the net tritium-breeding ratio be $\Lambda \equiv \mathrm{TBR}$; self-sufficiency with a realistic inventory and recycling requires $\Lambda \ge \Lambda_{\min} \approx 1.05$ [10]. The literal frozen blanket recipe gives a baseline $\Lambda_0$ that is fragile against the beryllium multiplier packing fraction $f_{\rm Be}$, i.e. $\partial\Lambda/\partial f_{\rm Be}$ is large. We stack $N$ *multiplier-independent* levers — outboard-blanket thickness, a sacrificial inboard liner, lithium-6 enrichment, and a reflector — each contributing a first-order fractional uplift $\delta_i$. Because the levers compete for the same finite neutron budget, their combination is sub-additive:

$$\Lambda(\quad\delta) = \Lambda_0 + \sum_{i=1}^{N} a_i\,\delta_i - \sum_{i<j} b_{ij}\,\delta_i\delta_j + \mathcal{O}(\delta^3), \qquad b_{ij} \ge 0,$$

so the linearised sum is a rigorous *upper* bound,

$$\Lambda(\quad\delta) \;\le\; \Lambda_0 + \sum_{i=1}^{N} a_i\,\delta_i \;\equiv\; \Lambda_{\rm ub}.$$

The point of the stack is that $\Lambda_{\rm ub}$ is achieved with a *demonstrated* $f_{\rm Be}$, i.e. the closure no longer depends on an unproven multiplier fraction; the honest statement is the bound $\Lambda \le \Lambda_{\rm ub}$, not a banked $\Lambda$.

## BREEDER GATE W3: MATERIALS-TESTING RATE AND STANDOFF GEOMETRY

The device is a high-fluence *volume* source rather than a high-rate point source. The wall-loading-anchored displacement rate at the first wall is

$$\dot D_{\rm FW} = \frac{\sigma_{\rm dpa}}{\bar A_{\rm cell}}\,\Gamma_n\big|_{\rm FW} \;\propto\; \Gamma_n\big|_{\rm FW} = \frac{P_n}{4\pi R_0^2\,\bar E_n}\,\eta_{\rm geo}(1),$$

with $\sigma_{\rm dpa}$ the NRT displacement cross-section [12] and $\Gamma_n$ the fast-neutron current. A re-entrant test port places specimens at a reduced standoff $d < d_{\rm FW}$, where the flux from the extended source scales as $\Gamma_n(d) = \Gamma_n\big|_{\rm FW}\,(d_{\rm FW}/d)^n$ with a geometric exponent bounded between $n = 1$ (a line/volume source) and $n = 2$ (a point source). A conservative bound takes $n = 1$, giving a re-entrant damage rate $\dot D(d) = \dot D_{\rm FW}(d_{\rm FW}/d)$ without any change to the mission power $P_{\rm fus}$. The competing lever — raising $I_p$ to raise $S_n$ — does raise the rate but trades centrepost life through the fast fluence, and is reported as a conditional negative rather than promoted [36].

## BURNER GATE: THE PLUG-DENSITY RATIO, THERMAL BARRIER, AND CENTRIFUGAL ALTERNATIVE

The tandem-mirror ion-confining potential $\phi_i$ is held by a plug whose electron population obeys the Boltzmann relation along the field line; with a plug electron temperature $T_e$ the required plug-to-central density ratio is

$$\frac{n_p}{n_c} = \exp\left(\frac{e\phi_i}{T_e}\right).$$

The frozen relation reproduces the design point at $n_p/n_c = 16$. Two independent levers act inside (14).

*Thermal barrier.* A hot-electron thermal barrier raises the carrier temperature that holds the potential from $T_e$ to $T_b > T_e$ [16], so at fixed $\phi_i$

$$\left.\frac{n_p}{n_c}\right|_{\text{barrier}} = \exp\left(\frac{e\phi_i}{T_b}\right) = \left(\frac{n_p}{n_c}\right)^{T_e/T_b}, \qquad \frac{T_b}{T_e} = \frac{\ln(n_p/n_c)}{\ln\left[(n_p/n_c)|_{\text{barrier}}\right]}.$$

Lowering the requirement from $16$ to $3.5$ therefore needs $T_b/T_e = \ln 16/\ln 3.5 \approx 2.2$ — a barrier electron population about twice as hot as the central electrons.

*Centrifugal rotating mirror.* An alternative supplies axial confinement by supersonic $E \times B$ rotation rather than by an electrostatic plug. An ion of mass $M$ rotating at angular frequency $\Omega = E_r/(rB)$ sees a centrifugal potential well of depth

$$\Phi_{\text{cf}} = \tfrac{1}{2} M\,\Omega^2 \left(R_{\max}^2 - R_{\min}^2\right),$$

between the large- and small-radius ends of a field line, and the effective confinement is set by the augmented factor $\exp(\Phi_{\text{cf}}/T_i)$. When $\Phi_{\text{cf}} \gtrsim \text{several} \times T_i$ — equivalently a rotation Mach number $M_s = v_{\text{rot}}/c_s \gtrsim$ a few — the rotation itself confines the ions and the electrostatic density-ratio gate is removed, $n_p/n_c \to 1$. The cost is a new gate: reactor-scale supersonic rotation and its interchange stability, which we carry openly in §6. A third, ruled-out lever — a higher-field plug coil — does not reduce the $\phi_i$ requirement of (14) and only raises magnet stress, and is reported as a negative.

§ 3

# Computational methodology: the NVIDIA GPU HPC campaign

## THE REDUCED-ORDER GATE EVALUATOR AND ITS DISCRETISATION

The screening surrogates $g_k^{\mathrm{RO}}$ are evaluated by the Kronos Research Toolkit, a physics engine that solves the 0-D/1-D balances underlying each gate. The breeder power/particle balance is a fixed-point problem $\vec{x} = \mathcal{T}(\vec{x})$ in the state $\vec{x} = (n_e, T, I_p, \ldots)$ whose converged root reproduces the frozen anchors $Q = 3.076$, $P_{\mathrm{fus}} = 85.04\,MW$, $I_p = 9.66\,MA$ (serial BR–L1–A1); Picard iteration is declared converged at a relative residual $\|\vec{x}^{(k+1)} - \vec{x}^{(k)}\|_\infty / \|\vec{x}^{(k)}\|_\infty < 10^{-6}$. The burner balance is the 0-D tandem-mirror Pastukhov-plug power balance reproducing $Q_E = 1.318$, $P_{\mathrm{fus}} = 4298.5\,MW$, $P_n = 233.95\,MW$ (serial BU–L1–A1), benchmarked against the WHAM operating point [21,15]. Each gate function $g_k^{\mathrm{RO}}$ is assembled from these balances plus the analytic relations of §2.

## THE ADVERSARIAL MIN–MAX SEARCH AND ITS CONVERGENCE

The bottleneck program (4) is solved on the design manifold $\{\vec{a}(\vec{p}) = \vec{a}_0\}$ by a projected search that alternates (i) a Latin-hypercube plus Sobol/Saltelli sampling of $\mathcal{P}$ to seed the binding set, and (ii) a derivative-free bottleneck ascent (Nelder–Mead with a margin-equalisation schedule) that lifts the active gates jointly. First-order and total Sobol sensitivity indices rank the levers and are converged on a $4 \times 10^4$-sample Monte-Carlo design (serials HX–05, KX–L1–A5): on the burner side the plug-density ratio is the first-order driver of $Q_E$ ($S_1 = 0.41$) and interacts strongly with the central beta ($S_T = 0.87$); on the breeder side confinement controls the gain variance ($S_1 = 0.885$, HX–03). Convergence of the min–max is declared when the spread of the active-set margins falls below $10^{-3}$ (margin equalisation) and the Sobol indices are stable to $\pm 0.02$ between successive sample doublings.

## HIGH-FIDELITY ANCHORS ON THE GPU HPC CAMPAIGN

The screening bounds are verified against high-fidelity calculations run on the NVIDIA GPU HPC campaign, which supplies the physics that the reduced-order gates are built to bound conservatively:

**Nonlinear gyrokinetics (CGYRO)** [23,24] confirms the negative-triangularity turbulence suppression that underwrites the confinement anchor: converged ion-scale runs give a suppression of $38$–$42\%$ (serial BR–L2–A1c), electron-scale (ETG) runs $79$–$80\%$ (REG–P13), and the advantage is robust across collisionality ($56$–$66\%$ over $\nu^* \times [0.25, 4]$, BR–L2–A13); deep-negative-triangularity ($\delta = -0.50$) turbulence was run once on an $8\times$ A100-80GB cluster (BR–CX–03). The GPU-resident spectral gyrokinetic solver is what makes converged, real-electron-mass multiscale reach affordable.

**Monte-Carlo neutron transport (OpenMC/DAGMC)** [25] supplies the tritium anchors underlying W2: a 3-D balance with leakage $0.121$ and net $\mathrm{TBR} = 1.026$ for the literal recipe (BR–L1–A5), and a CAD-faithful centrepost scan with net $\mathrm{TBR} = 1.0537$ and life $0.199$ fpy (BR–SX–12), event-based on GPU.

**Particle-in-cell (WarpX)** evaluates the plug microstability at $n_p/n_c = 16$: the DCLC loss-cone mode is bare-unstable but stabilised by a maintained warm-plasma fraction (HX–23, BU–L2–A7), a GPU PIC result that bounds the plug operating point the burner gate depends on.

**Free-boundary equilibrium** [26] provides the poloidal-beta anchor $\beta_p = 0.371$ (BR–L1–A12) and the Troyon/kink margins ($\beta_N$ below the no-wall Troyon value $\approx 2.8$ with a binding external-kink margin $1.15$–$1.31\times$, BR–L2–A19) that set the $\beta$ headroom of W1. itemize

## VERIFICATION AND REPRODUCIBILITY

Every gate is reproduced by an independent library where one exists: the CGYRO linear spectrum is byte-identical to the bundled reference (BR–L2–A18b; $\gamma = +0.3179$ in $a$-units), and a quasilinear TGLF cross-check reproduces the CGYRO negative-triangularity suppression ($36.8\%$ mean, up to $60\%$; HX–17) [30]. The independent-library gate reproduction and the byte-for-byte provenance catalogue are documented in the companion verification papers [37,38]. The reduced-order evaluator, the min–max search, and the figure scripts are archived with this paper's deposit.

§ 4

# Results

## THE BINDING-MARGIN MAP

Figure 1 states the method and figure 2 its first output: the normalised gate margins at the frozen point. Three breeder gates and the burner plug gate fall at or below the pass threshold — the honest failure surface, located by (2). The current-drive gate binds hardest on the breeder ($P_{CD}/P_{fus} > 1$ maps to a margin $0.72 < 1$), tritium closure is marginal ($1.026$ against $1.05$), and the plug-density gate binds the burner. The remaining sections lift each in turn.

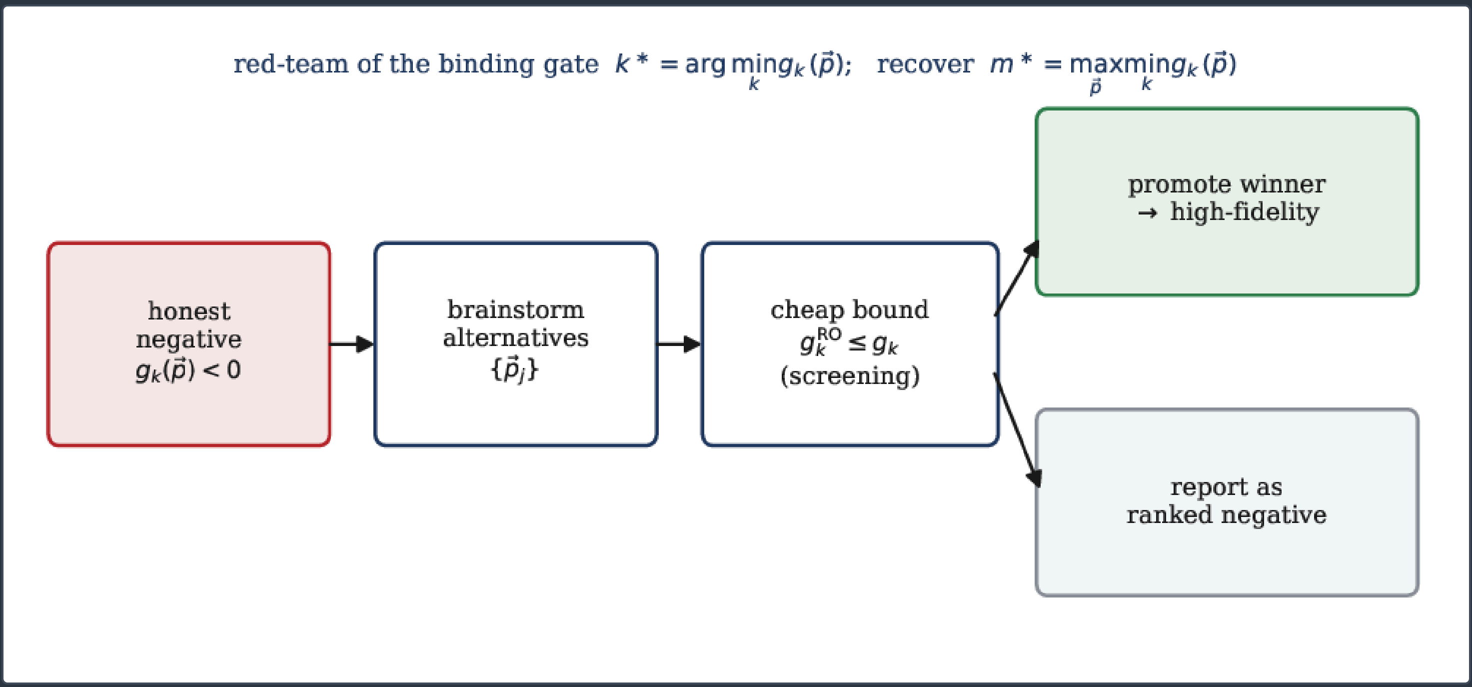


**(Schematic.)** The red-team method. For each honest negative $g_k < 0$ we brainstorm alternatives, bound each with a conservative reduced-order model satisfying the screening property $g_k^{RO} \leq g_k$ (equation 5), and either promote the winner to high-fidelity validation or report it as a ranked negative. The adversarial target is the binding gate $k^* = \arg\min_k g_k$ and the recovered value $m^* = \max_{\vec{p}} \min_k g_k$ of equation (3).

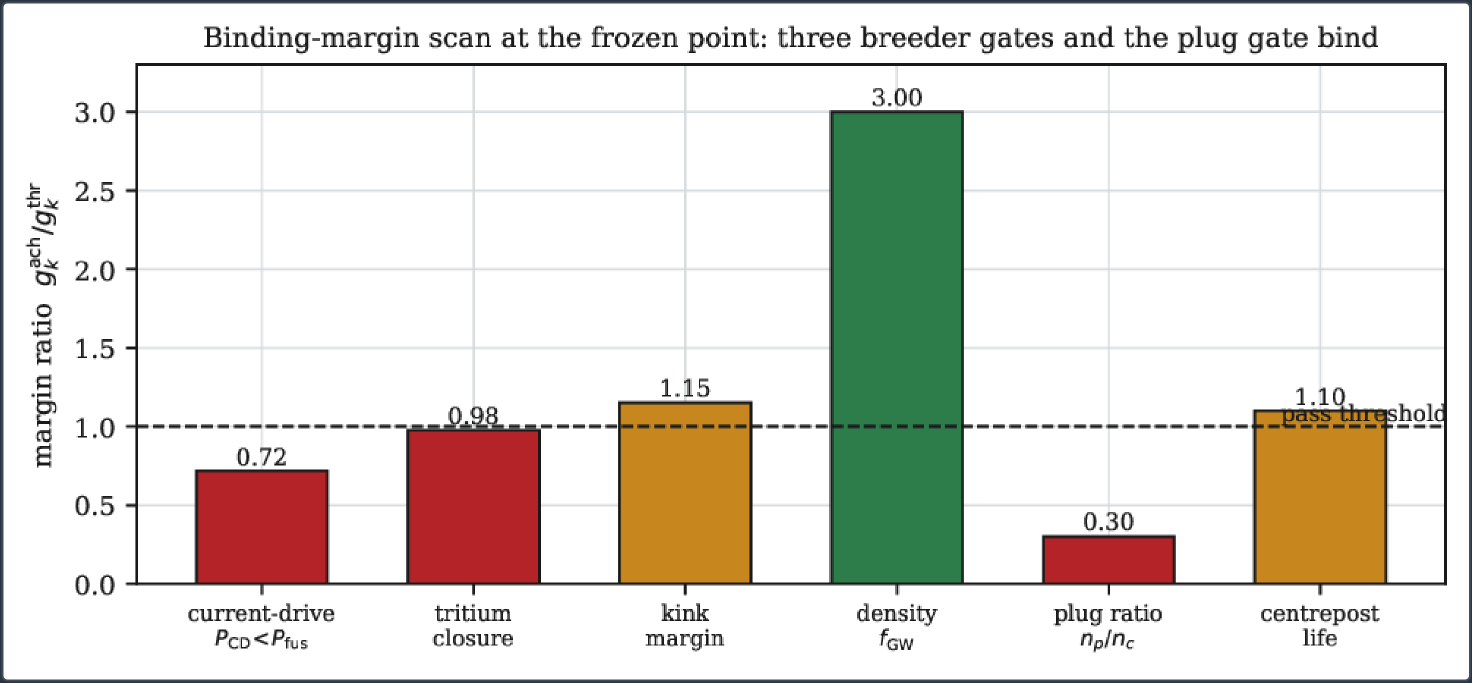


Binding-margin scan at the frozen design point (normalised achieved/threshold ratios; register serials in the text). Bars below the dashed pass line bind: the breeder current-drive gate (**0.72**), tritium closure (**0.98**), and the burner plug-density gate; the kink, density and centrepost-life gates clear. The smallest bar is the binding gate $k^*$ of equation (2).

## W1: CURRENT-DRIVE BURDEN VERSUS $\beta$-HEADROOM

The solenoid-free baseline sustains flat-top with $P_{CD} = 118.5\,MW$ of NBCD at a low bootstrap fraction $f_{bs} = 0.155$ (serials `BR-CX-07`, `BR-L2-A6`), which exceeds the fusion power $P_{fus} = 85.04\,MW$ — the honest negative. Moving to an advanced operating point inside the unused Troyon headroom raises $\beta_p$ from its baseline 0.371 (`BR-L1-A12`) along the bootstrap scaling of equation (8) (figure 3), lifting $f_{bs}$ toward $\approx 0.45$; the higher electron temperature simultaneously raises $\gamma_{CD}$. Evaluating the ratio (10) with $f_{bs} : 0.155 \to 0.45$, $\gamma_{CD}$ up $\approx 1.6\times$, and density up $\approx 1.15\times$ gives $P'_{CD}/P^0_{CD} \approx 0.42$, i.e. $P_{CD} \approx 50\,MW$ — below fusion power (figure 3) — while the neutron source rises by $1.68\times$ (figure 4). The advanced point uses 49% of the $\beta$ ceiling. The lever is unused pressure headroom, and the underlying confinement that makes the advanced point accessible is the de-risked negative-triangularity result [29].

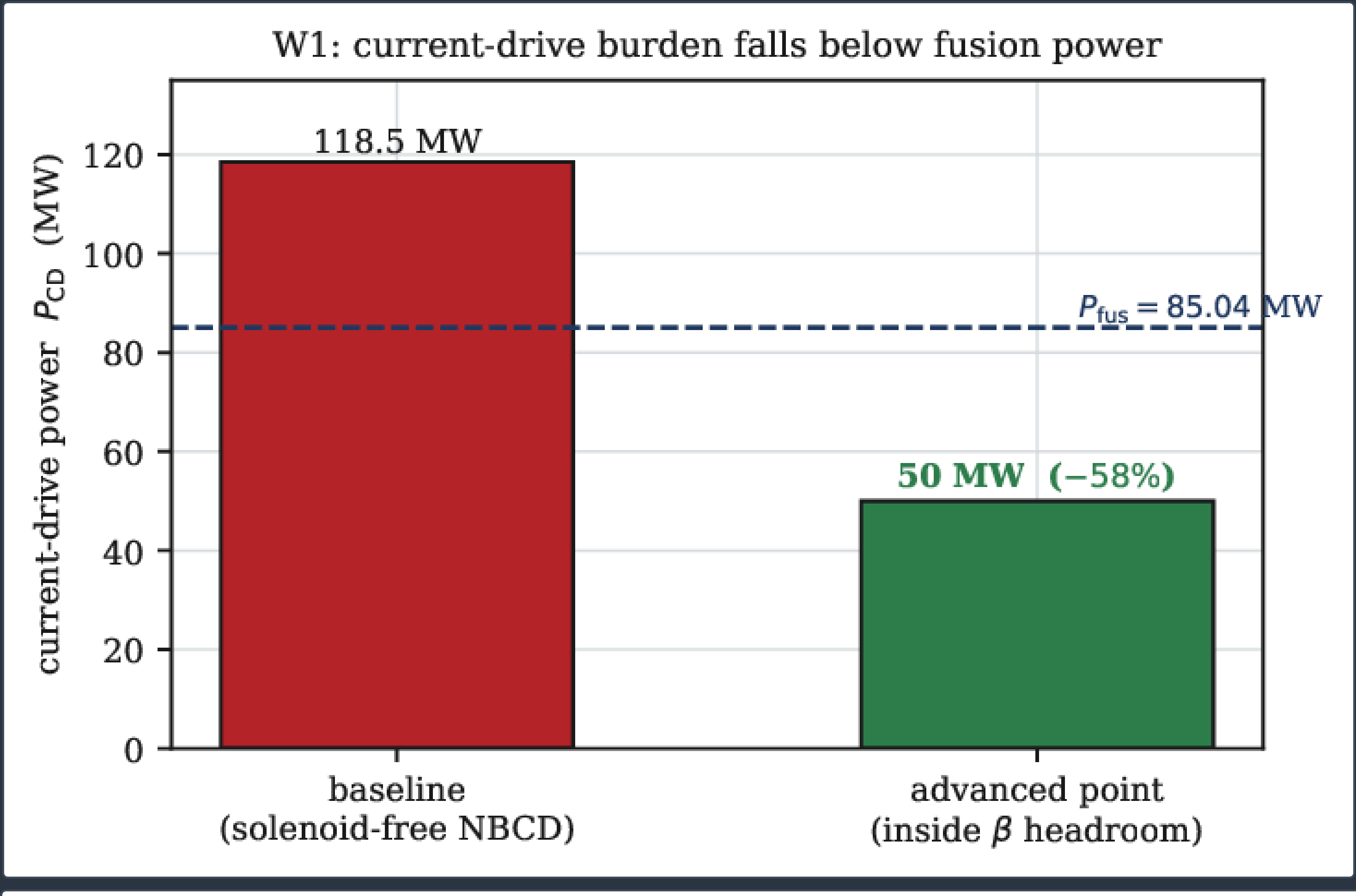
W1: current-drive burden falls below fusion power
current-drive power $P_{CD}$ (MW)
118.5 MW
$P_{fus} = 85.04$ MW
50 MW (−58%)
0
20
40
60
80
100
120
baseline
(solenoid-free NBCD)
advanced point
(inside $\beta$ headroom)

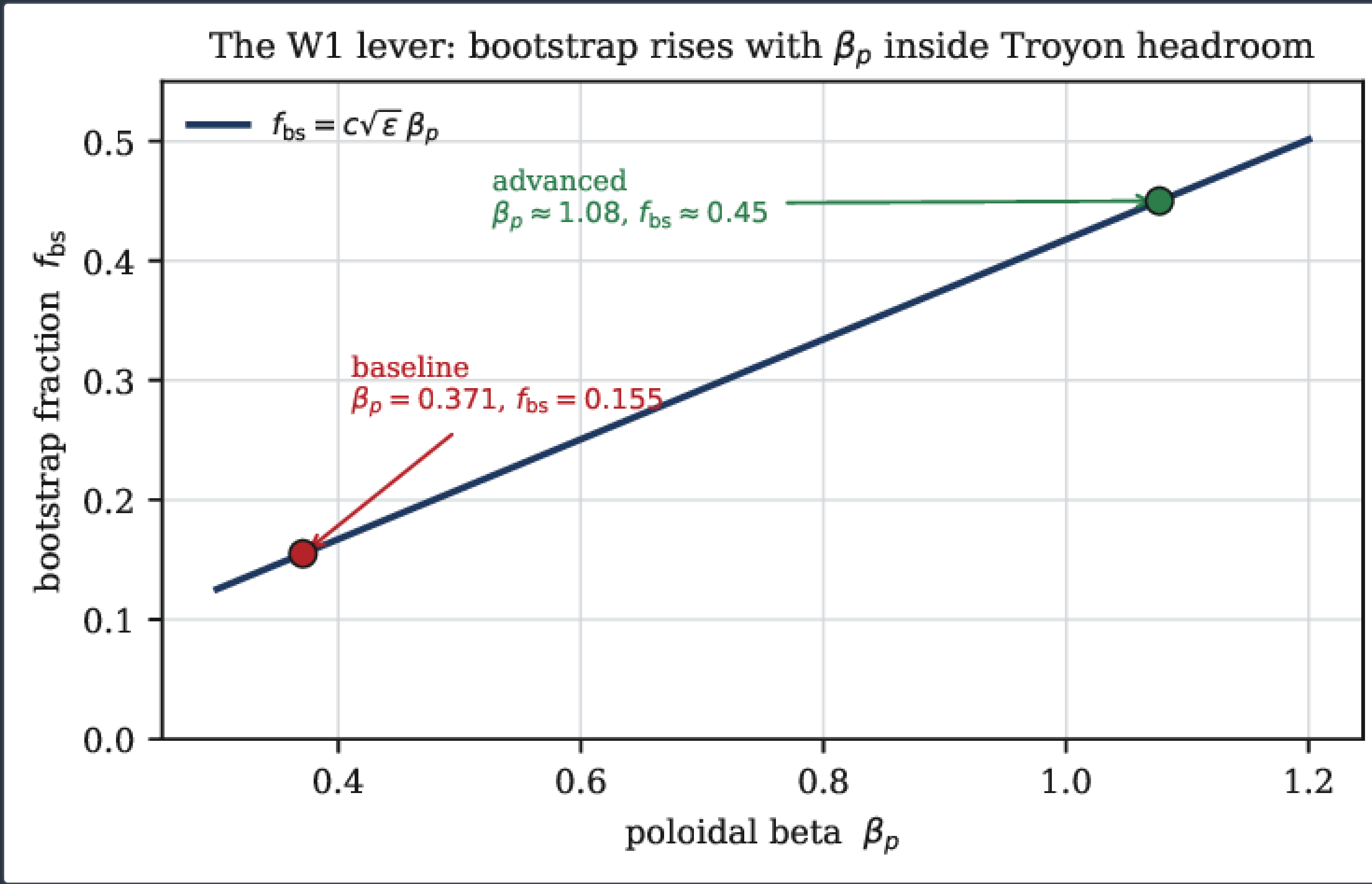
The W1 lever: bootstrap rises with $\beta_p$ inside Troyon headroom
$f_{bs} = c\sqrt{\varepsilon}\,\beta_p$
advanced
$\beta_p \approx 1.08$, $f_{bs} \approx 0.45$
baseline
$\beta_p = 0.371$, $f_{bs} = 0.155$
bootstrap fraction $f_{bs}$
0.0
0.1
0.2
0.3
0.4
0.5
0.4
0.6
0.8
1.0
1.2
poloidal beta $\beta_p$

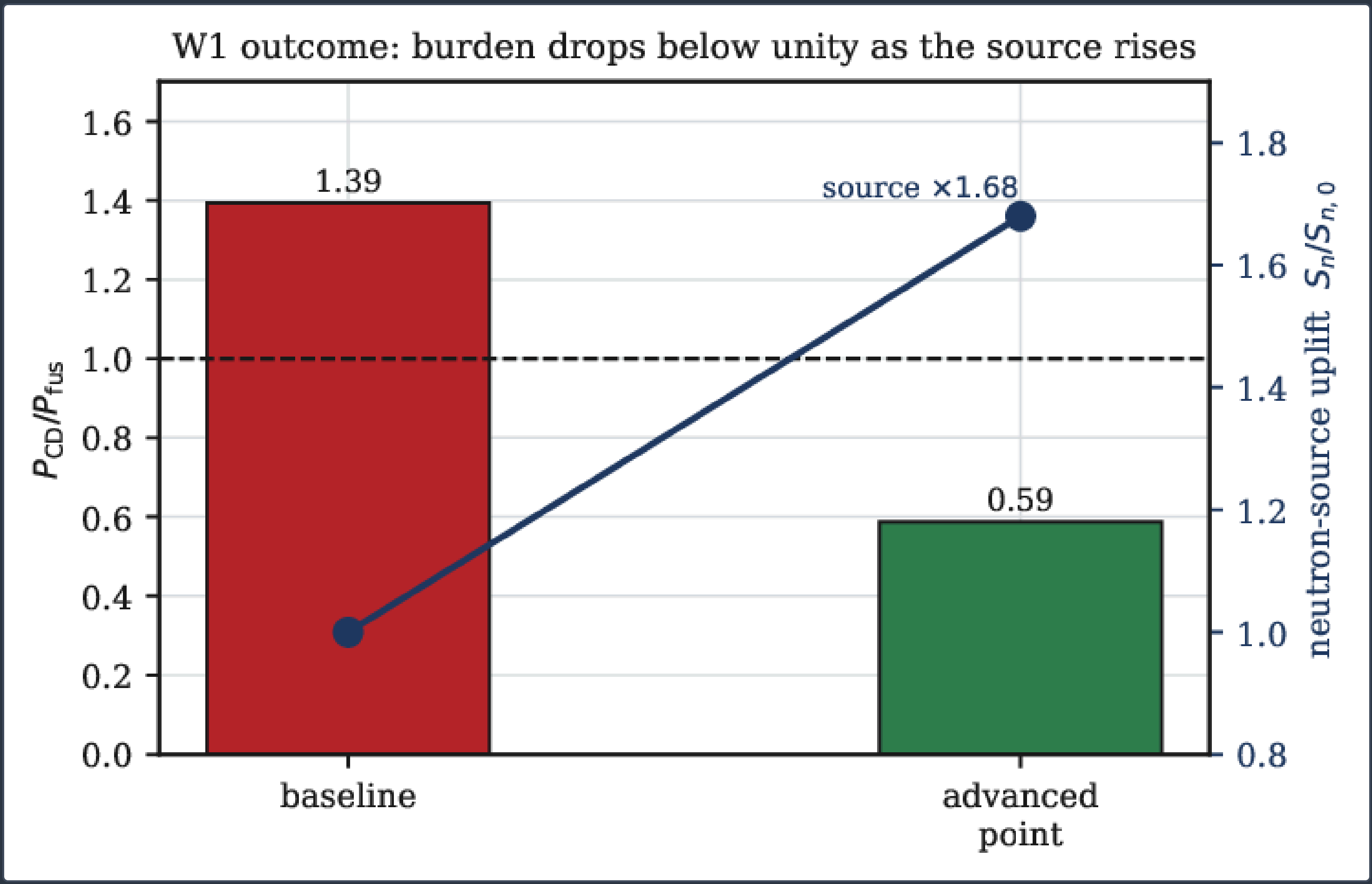


W1 in mission terms. The current-drive-to-fusion power ratio $P_{\mathrm{CD}}/P_{\mathrm{fus}}$ crosses below unity (left axis, bars) as the $14\,MeV$ neutron source rises by $1.68\times$ (right axis, line).

## W2: MULTIPLIER-INDEPENDENT TRITIUM CLOSURE

The literal recipe breeds $\Lambda_0 = 1.026$ (serials BR–L1–A5, BR–L2–A7), fragile against $f_{Be}$. Stacking the four multiplier-independent levers of equation (11) — with outboard thickness, a sacrificial inboard liner, lithium-6 enrichment, and a reflector — lifts closure along the sub-additive waterfall of figure 5 to the upper bound $\Lambda_{ub} = 1.204$ of equation (12), comfortably above the $\Lambda_{min} = 1.05$ self-sufficiency threshold and consistent with the blanket-thickness scan ($\Lambda = 1.2407$ at $65\,cm$, BR–L2–A11h) and the CAD centrepost result ($\Lambda = 1.0537$, BR–SX–12). The value is stated as a bound: the closure no longer depends on an unproven multiplier fraction [33].

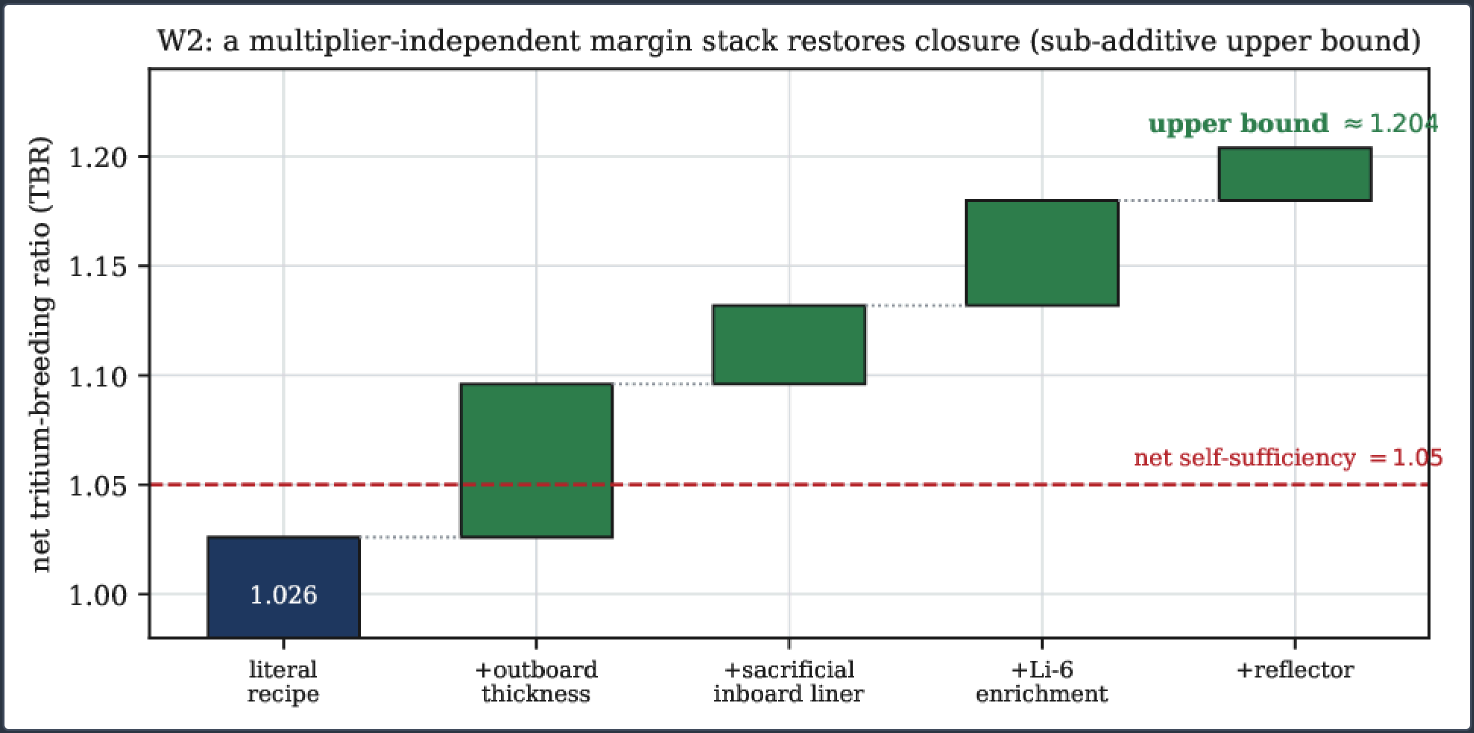


W2 outcome. A multiplier-independent margin stack (equation 11) lifts net TBR from the literal recipe $1.026$ to the sub-additive upper bound $\approx 1.204$, above the $1.05$ self-sufficiency line. Bars are stacked in first-order; the true combination is below the linear sum, so $1.204$ is an upper bound.

## W3: A REDUCED-STANDOFF MATERIALS-TEST PORT

At the first wall the wall-loading-anchored damage rate is [redacted] (serial BR–L1–A13), and the corrected wall value is [redacted] (BR–SX–02). A re-entrant port at reduced standoff reaches [redacted] on the conservative $n = 1$ geometric bound of equation (13) (figure 6) without changing mission power — the gain is modest precisely because the machine is already a high-fluence volume source rather than a point source. The competing lever, raising $I_p$, does reach a higher rate but consumes centrepost life through the fast fluence and is reported as a conditional negative, consistent with the lifetime-constrained operating window of the companion synthesis [36].

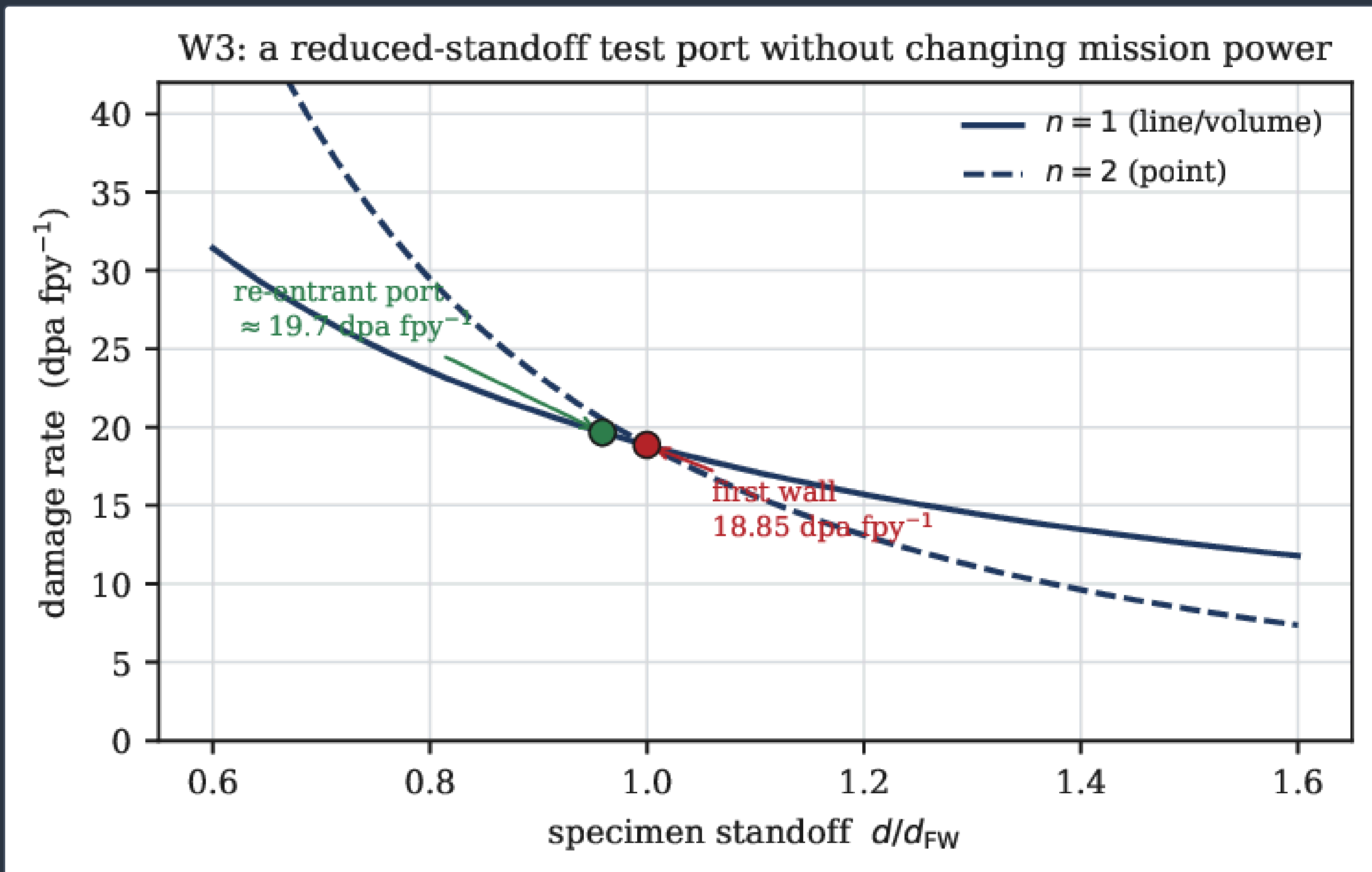


W3 outcome. Displacement rate versus specimen standoff from equation (13); the conservative $n = 1$ bound and the $n = 2$ point-source bound bracket the enhancement. A re-entrant port reaches [redacted] from the [redacted] first-wall rate without changing $P_{\text{fus}}$.

## THE BURNER PLUG-DENSITY GATE AND ITS ALTERNATIVES

The burner's entry gate is $n_p/n_c = 16$ from equation (14). Figure 7 shows the two promoted alternatives and figure 7 shows why 16 is a robust knee rather than the fragile steep zone: on the plug-ratio Pareto (serial AG–CX–02) the ion-confining potential $\phi_i$ saturates near $249\,keV$ by $R \approx 16$ while the gain $Q_E$ only begins to climb its cliff beyond it ($Q_E : 1.32 \to 2.7 \to 23$ over $R : 16 \to 20 \to 24$). The hot-electron thermal barrier acts inside the exponent of (14): by equation (15) a barrier-to-central temperature ratio $T_b/T_e \approx 2.2$ lowers the required density ratio to $\approx 3.5$ (figure 8), and the barrier's temperature lever is independently load-bearing — holding the central electron temperature at $\approx 90\,keV$ is worth $+2.8\times$ in $Q_E$ ($0.47 \to 1.318$, serial AG–CX–05) [34]. The centrifugal rotating-mirror architecture supplies axial confinement by the centrifugal potential of equation (16) and removes the density-ratio gate entirely ($n_p/n_c \to 1$), at the cost of the rotational-stability question of §6. Figure 9 collects the ranked verdicts. Table 1 summarises the four gates and table 2 the ranked alternatives; table 3 lists the frozen anchors and table 4 the verifying codes.

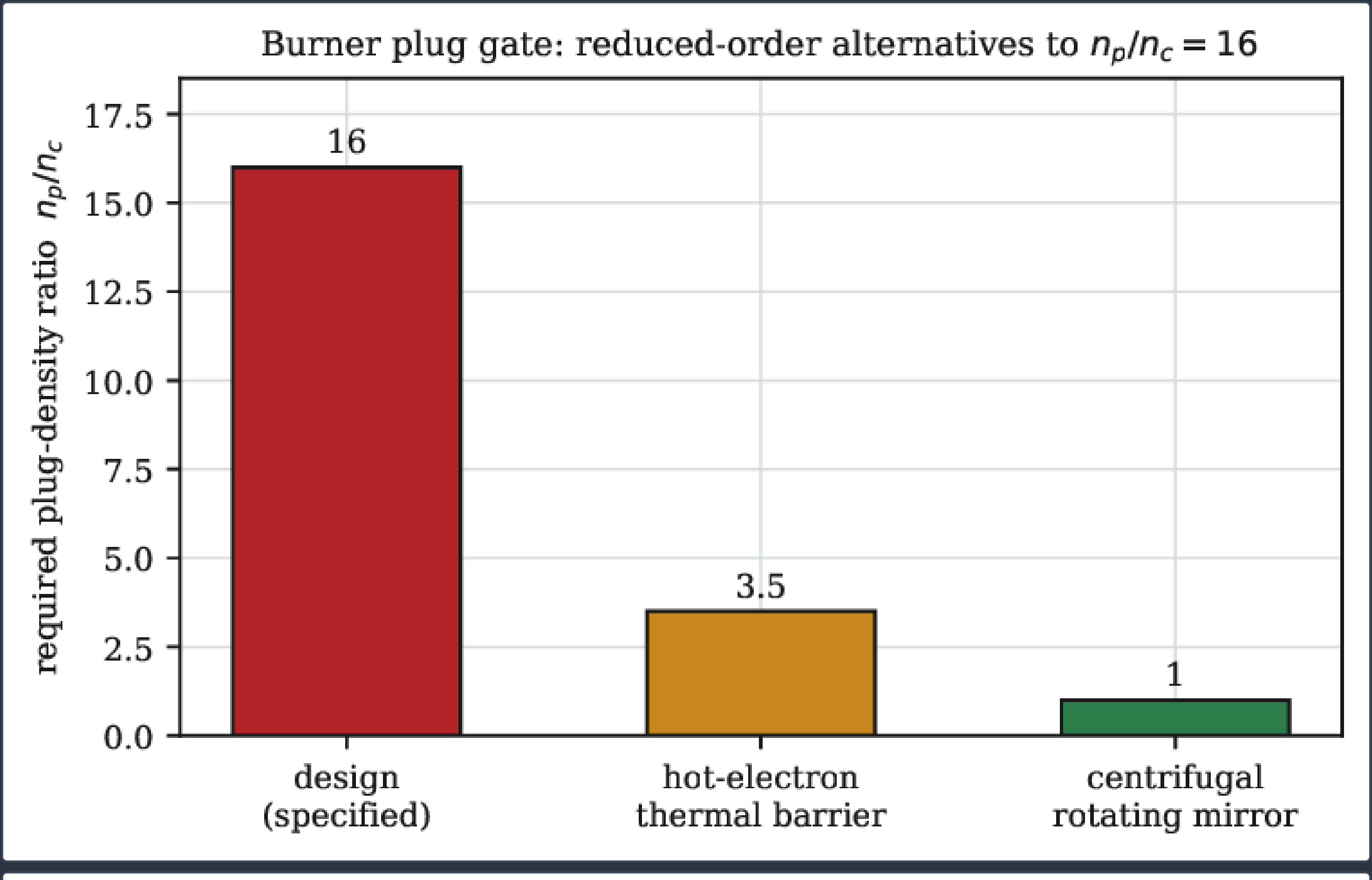


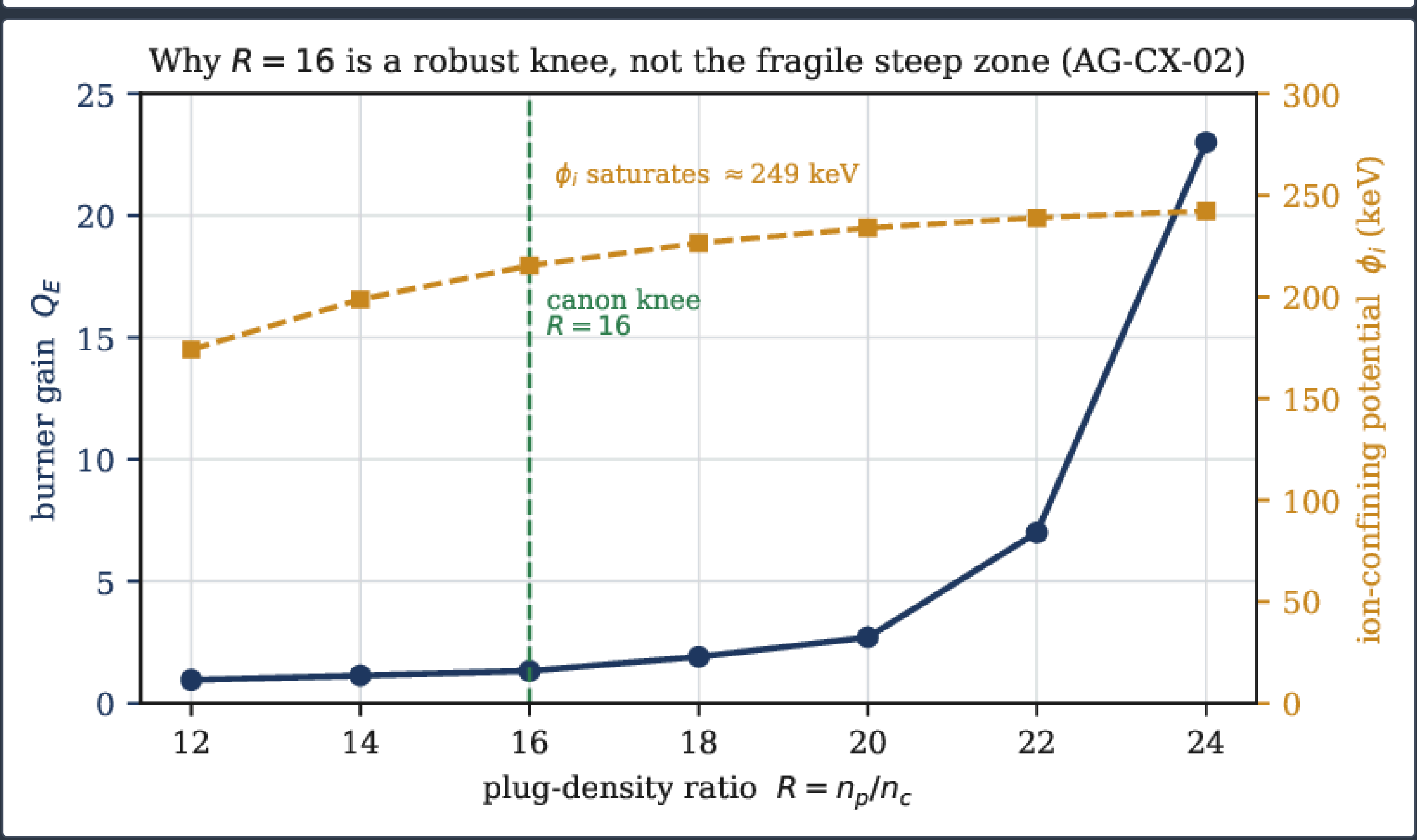


Burner plug-density alternatives (reduced-order screening). A hot-electron thermal barrier lowers the required $n_p/n_c$ from 16 to ≈ 3.5 (equation 15); a centrifugal rotating mirror removes the gate (≈ 1.0, equation 16).

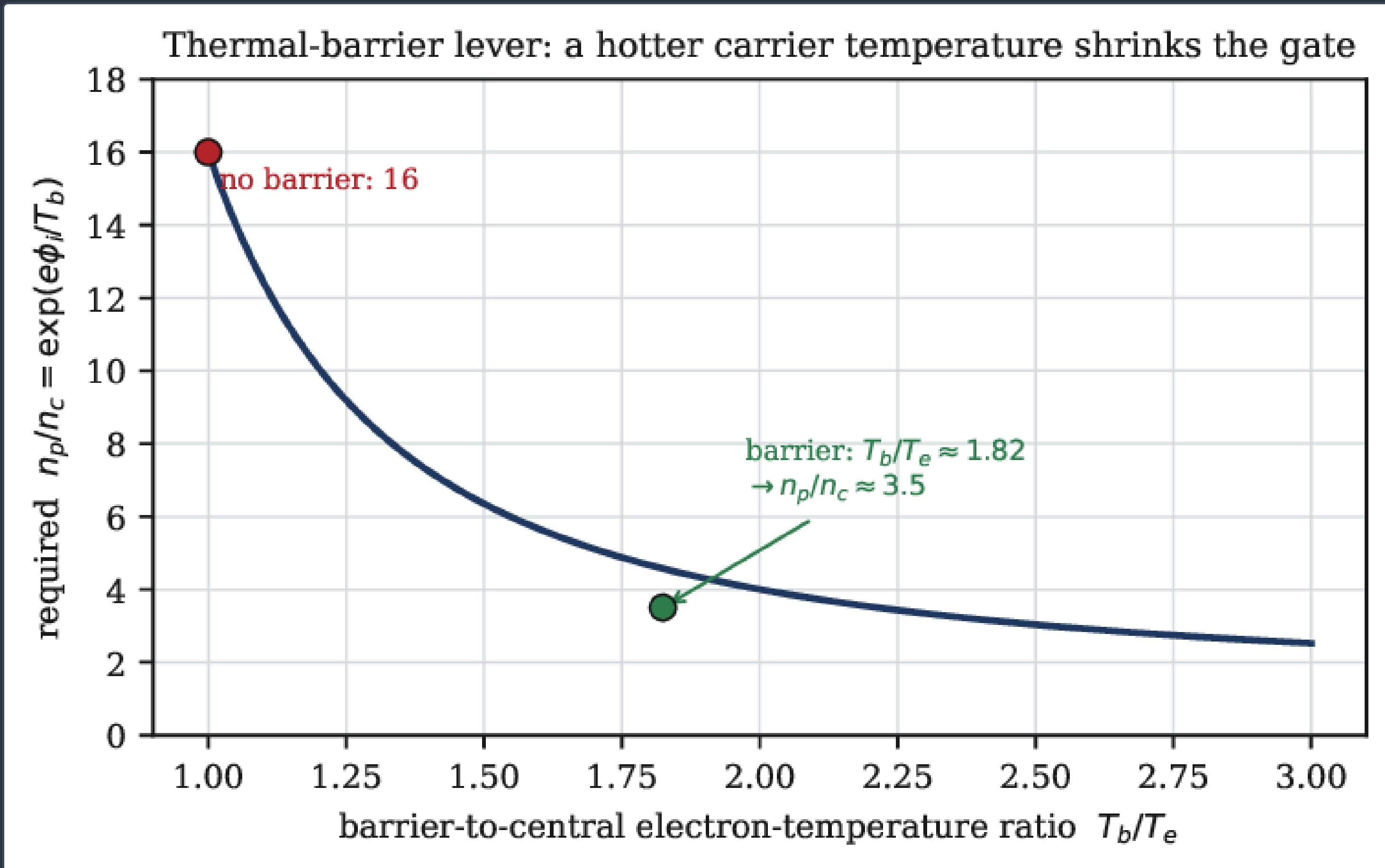


The thermal-barrier lever of equation (15). The required $n_p/n_c = \exp(e\phi_i/T_b)$ falls as the barrier-to-central electron-temperature ratio $T_b/T_e$ rises; $T_b/T_e \approx 2.2$ takes the requirement from $16$ to $\approx 3.5$.

Ranked-alternative decision map: promoted paths vs reported negatives

| gate | screened alternative | verdict |
|---|---|---|
| W1 current drive | advanced $\beta$-headroom point | PROMOTE |
| W2 tritium | multiplier-independent stack | PROMOTE |
| W3 test rate | reduced-standoff re-entrant port | PROMOTE |
| W3 (alt) | raise $I_p$ (trades centrepost life) | REPORT NEG. |
| plug gate | hot-electron thermal barrier | PROMOTE |
| plug gate | centrifugal rotating mirror | PROMOTE* |
| plug gate (alt) | higher-field plug coil | RULED OUT |

*PROMOTE with an open rotational-stability gate (Limitations).

**(Schematic.)** Ranked-alternative decision map. Promoted paths (green) go to high-fidelity validation; reported negatives (grey) and the ruled-out higher-field plug coil are recorded, not hidden. The centrifugal mirror is promoted with an open rotational-stability gate (asterisk; §6).

| GATE | MACHINE | HONEST NEGATIVE | CLOSING LEVER | SCREENING BOUND |
|---|---|---|---|---|
| **W1 current drive** | breeder | $P_{CD} = 118.5\,MW > P_{fus}$ | advanced $\beta$-headroom point | $P_{CD} \to 50\,MW$ ($-58\%$) |
| **W2 tritium** | breeder | closure fragile in $f_{Be}$ | multiplier-independent stack | TBR $\leq 1.204$ |
| **W3 test rate** | breeder | volume, not point, source | reduced-standoff port | [redacted] |
| **plug density** | burner | $n_p/n_c = 16$ | thermal barrier / centrifugal | $\to 3.5$ / $\to 1.0$ |

The four binding gates, the closing lever, and the screening-bound outcome. Serials refer to the de-risking register [28]. Every outcome is a reduced-order screening bound, not a banked result.

| GATE | ALTERNATIVE | BASIS | VERDICT |
|---|---|---|---|
| **W1** | advanced $\beta$-headroom operating point | eqs. (8)–(10); BR–L2–A19 | **promote** |
| **W2** | outboard/liner/$^6$Li/reflector stack | eq. (12); BR–L2–A11h | **promote** |
| **W3** | reduced-standoff re-entrant port | eq. (13); BR–SX–02 | **promote** |
| **W3** | raise $I_p$ for higher source | trades centrepost life; KX–L1–A21 | report negative |
| **plug** | hot-electron thermal barrier | eq. (15); AG–CX–05 | **promote** |
| **plug** | centrifugal rotating mirror | eq. (16); AG–DR–03 | promote* |
| **plug** | higher-field plug coil | no $\phi_i$ reduction; raises stress | ruled out |

Ranked alternatives per gate and verdict. “Promote” sends the lever to high-fidelity validation; “report negative” and “ruled out” are recorded, not hidden.

| QUANTITY | VALUE | SERIAL |
|---|---|---|
| **breeder gain $Q$** | 3.076 | BR–L1–A1 |
| **breeder fusion power $P_{fus}$** | 85.04 MW | BR–L1–A1 |
| **breeder plasma current $I_p$** | 9.66 MA | BR–L1–A1 |
| **triangularity / elongation** | $\delta = -0.30$, $\kappa = 2.0$ | BR–L1–A7 |
| **on-axis field / aspect ratio** | $B_0 = 8\,T$, $A = 2.5$ | BR–L1–A7 |
| **centrepost peak field** | 16.84 T | KX–L1–A15 |
| **baseline bootstrap fraction $f_{bs}$** | 0.155 | BR–L2–A6 |
| **baseline poloidal beta $\beta_p$** | 0.371 | BR–L1–A12 |
| **burner gain $Q_E$** | 1.318 | BU–L1–A1 |
| **burner neutron fraction $f_n$** | 5.44% | ENV–A2–BU |
| **burner plug field** | 26.49 T | KX–L1–A15 |
| **direct-conversion efficiency $\eta_{DEC}$** | 0.49 | ADJ3 |

Frozen design anchors used in this red-team (register [28]). The breeder centrepost and the burner plug are two distinct magnets and are never conflated.

| CODE | ROLE | GATE SUPPORTED | SERIAL |
|---|---|---|---|
| **CGYRO** [23] | nonlinear gyrokinetics (NT suppression) | W1 confinement basis | BR–L2–A1c |
| **OpenMC/DAGMC** [25] | Monte-Carlo neutron transport | W2 tritium | BR–L1–A5 |
| **WarpX** | particle-in-cell plug microstability | burner plug | HX–23 |
| **FreeGS** [26] | free-boundary equilibrium | W1 $\beta$ headroom | BR–L1–A12 |
| **TGLF** | quasilinear cross-check | confinement verify | HX–17 |

High-fidelity codes on the NVIDIA GPU HPC campaign that verify the screening bounds, with the gate each supports and the anchoring serial.

§ 5

# Discussion

The four closures should be read against the published literature that motivates each gate.

*Current drive.* That a low-bootstrap, solenoid-free ST needs current-drive power comparable to or exceeding fusion power is exactly the tension the advanced-tokamak programme was built to relieve by aligning a high bootstrap fraction with efficient off-axis drive [6,7]. W1 is a quantitative instance: raising $\beta_p$ into the Troyon headroom [8] lifts $f_{\mathrm{bs}}$ from $0.155$ toward $\approx 0.45$ and, with the temperature dependence of $\gamma_{\mathrm{CD}}$, drops $P_{\mathrm{CD}}$ below $P_{\mathrm{fus}}$. The move is legitimate only because the confinement at the advanced point is itself de-risked: nonlinear CGYRO shows the negative-triangularity quiescence survives at ion and electron scales [29,30,4,5], so the higher-pressure point is not bought with a turbulence penalty.

*Tritium.* Compact devices sit on the tritium knife-edge, and the required margin against inventory and recycling is the classic self-sufficiency window of Sawan and Abdou [10,11]. W2's contribution is to make the closure *multiplier-independent*: the sub-additive bound of equation (12) reaches $\Lambda_{\mathrm{ub}} = 1.204$ with a demonstrated beryllium fraction, so the closure no longer hangs on an unproven $f_{\mathrm{Be}}$ [33].

*Materials testing.* The device is a volume source; its first-wall dpa rate ([redacted]) is prototypical in spectrum and competitive in rate with dedicated fusion-materials-source concepts, and the standard NRT convention [12,13] makes the number comparable across facilities. W3 shows the re-entrant port captures the wall flux without a mission-power change, and honestly reports the higher-$I_p$ alternative as a life-trading negative [36].

*Plug density.* The plug requirement descends from Pastukhov ambipolar theory [14,15]; the frozen $n_p/n_c = 16$ is the robust knee of the Pareto (figure 7), not the fragile steep zone. The thermal-barrier lever is the same physics that Baldwin and Logan introduced to decouple the plug electron population [16,17,18], now confirmed as load-bearing on the Kronos burner ($+2.8\times$ $Q_E$) [34]; and modern axisymmetric mirrors such as WHAM report the hot-electron and temperature gains the barrier relies on [21,22]. The centrifugal alternative has its own experimental lineage — the Maryland Centrifugal Experiment demonstrated steady supersonic rotation [20], and rotating-mirror reactor studies date to Bekhtenev [19] — so removing the electrostatic gate by rotation is grounded, with the reactor-scale stability question the honest open item.

§ 6

# Limitations

The one honest gate this analysis opens rather than closes is the rotational (interchange) stability of the centrifugal alternative at reactor scale. Removing the electrostatic plug by supersonic rotation (equation 16) trades a known gate for a new one: the central cell of the mirror is interchange-unstable when unrotated (serial `AG–DR–03`, $a/\rho \approx 144$), and while the central beta $\beta_c = 0.55$ sits $\times 1.82$ below the hard $\beta = 1$ limit, the velocity-shear and curvature balance that must stabilise a reactor-scale supersonically rotating column is not resolved by a reduced-order model and is the subject the high-fidelity follow-on must address. More generally, every headline in this paper is a reduced-order screening bound satisfying (5): the W1 advanced point awaits a self-consistent transport-and-current-drive calculation, the W2 stack awaits three-dimensional neutronics, and the plug alternatives await kinetic and stability validation. None is a banked result.

§ 7

# Conclusion

Casting the red-team as a min–max over the frozen design point (equations 1–4) locates the binding gates and quantifies how far each can be recovered under fixed mission anchors. Three breeder gates and the burner plug gate bind, and each has a bounded, named closing path. The current-drive burden falls from $118.5\,MW$ to $50\,MW$ ($-58\%$, below the $85.04\,MW$ fusion power) at an advanced operating point inside unused Troyon headroom, with the source up $1.68\times$; tritium closure is restored to a multiplier-independent upper bound $\mathrm{TBR} \leq 1.204$ above the $1.05$ self-sufficiency threshold; a reduced-standoff port reaches [redacted] without changing mission power; and the burner plug requirement falls from $n_p/n_c = 16$ to $\approx 3.5$ with a thermal barrier or $\approx 1.0$ with a centrifugal rotating mirror. These are screening bounds that direct high-fidelity validation, not banked results — but they show the honest negatives are closable, and they name where the levers were hiding: in unused design headroom, not in new physics.

Acknowledgments tocsectionAcknowledgments Part of the Kronos Fusion Energy 2026 design series. The author thanks the Kronos physics de-risking programme for the frozen result set underlying every quantitative claim, and the negative-triangularity confinement team whose de-risked result makes the advanced current-drive point admissible.

Reproducibility. Every headline quantity is a frozen anchor in the Kronos Physics De-Risking Register [28] (the de-risking register, doi:10.5281/zenodo.22133057) and is regenerable from the archived reduced-order evaluator, the min–max search, and the figure-generation script deposited with this paper. This paper is archived at doi:10.5281/zenodo.22645720 and its official page is https://www.kronos-fusionenergy.com/publications/red-team-of-the-binding-gates.html. No result depends on unpublished or proprietary data.

Scope — what this paper does not claim. These are reduced-order screening bounds and ranked alternatives, not banked high-fidelity results; each promoted path is a candidate for validation, and only after that validation is a number banked.

Data availability tocsectionData availability The reduced-order screening models, the ranked-alternative records, and the figure data used for figures 2–8 are archived with the deposit for this paper at doi:10.5281/zenodo.22645720. All quantitative values trace to the register [28] by the serial identifiers cited inline, and cross the Kronos 2026 series through the companion papers [29,31,32,33,34,35,36,30]. Any economic analysis is reported separately and is not part of the public deposit.

Competing interests tocsectionCompeting interests The author is affiliated with Kronos Fusion Energy. Provisional patent applications relating to aspects of this work have been filed.

tocsectionReferences

APPARATUS

# *Portfolio, People & Record*

*The intellectual-property estate, the people who built it, the limitations that gate it, and the sources it rests on.*

| | | | |
|---|---|---|---|
| 1 | 4 | 40 | 27 |
| GRANTED PATENT | 2026 PROVISIONALS | TEAM MEMBERS | 2022 PROVISIONALS |

INTELLECTUAL PROPERTY

# The patent portfolio

The estate spans a granted high-field magnet patent, pending utility and 2026 provisional filings that map to the two products, a digital-twin control provisional, a registered trademark application, and the original 2022 provisional family. Every patentable disclosure in the five-paper arXiv drop was protected **before** publication: the breeder and burner provisionals were filed 1–2 August, and a publication-gap omnibus filing the evening before the drop swept up the DEC, plasma-control, and REBCO-winding matter of the three otherwise-unprotected papers. Patent numbers and application serials are matters of public record; claim scope is summarised, not reproduced.

## GRANTED & PENDING UTILITY

| | | |
|---|---|---|
| US 12,009,112 | High-field tilted graded-REBCO magnet architecture (KRONO-002A) · *app. 17/878,550* | GRANTED |
| US 17/878,507 | Core device / method (KRONO-001A) · *utility* | PENDING |

## 2026 PROVISIONAL FILINGS — MAPPED TO THE PRODUCTS

| | | |
|---|---|---|
| 64/124,209 | Hyperion — spherical-tokamak tritium / helium-3 foundry · *breeder · filed Aug 2026* | FILED |
| 64/124,220 | Aegis / MetroVolt — synchrotron-cutoff, fuel-selection & plug-winding · *generator · filed Aug 2026* | FILED |
| 64/115,167 | KRONOS-CTRL digital-twin plant control · *provisional · filed Jul 2026* | FILED |
| 64/005,440 | Integrated spherical-tokamak fusion architecture · *early integrated-architecture filing · filed Mar 2026* | FILED |
| 64/105,530 | Negative-triangularity spherical-tokamak architecture · *foundational ST filing · filed Jul 2026* | FILED |
| 64/128,097 | Publication-gap omnibus — quasineutral two-species expander DEC · provenance-gated / latency-split plasma control · as-built high-field winding & conductor architecture · *filed 7 Aug 2026, the evening before the arXiv drop* | FILED |

## TRADEMARK & ORIGIN

| | | |
|---|---|---|
| FTK-98801894 | Kronos Fusion Energy — trademark application | FILED |
| KR-2022-* | Original provisional family (KR-2022-00001 … 00027) · *27 filings, 2022* | PRIORITY |

The narrow, defensible magnet novelty — the specific conductor and the digital-twin winding optimisation, not high-field REBCO as a category — is the commercial core that can earn ahead of any Q > 1 milestone, with markets in fusion magnet supply, MRI/NMR, accelerators, and proton therapy. The claim is scoped honestly: the high field is a *system field* result, not a stand-alone-coil record; the small-bore plug coil is structurally infeasible as a bare winding but resolved by a stress-managed structural shield (feasible-pending-FEA); and the winding-tape experiment returned a *null result*. The value is the method, not a field record.

THE TEAM

# Founding partners, board, advisors & auditors

Kronos is built by a bench of advanced-fuel-fusion, high-field-magnet, direct-conversion, and materials specialists, with a board and operations team drawn from defense, national laboratories, and industry. Dates are shown as ranges; where a tenure has ended or is term-ending, the range says so.

## FOUNDING PARTNERS — SCIENCE

**Dr. Gerald Kulcinski**
Co-Founder · Helium-3 & Advanced-Fuel Fusion
*UW–Madison · 2023–Present*

**Dr. Carl Weggel**
Chief Scientist / S.M.A.R.T. Design
*MIT Alcator Program · 2022–Present*

**Dr. Robert J. Weggel**
Magnetic Field Design
*MIT Magnet Lab · 2022–Present*

## BOARD

**Priyanca Ford**
Founder & CEO · Executive Board
*2022–Present*

**Bandel Carano**
Finance / Strategy
*Oak Investment Partners / Stanford · 2025–2026*

**Patrick Schweiger**
Fusion Device Engineering
*Oklo / CFS / TerraPower · 2025–Present*

## SCIENTIFIC ADVISORS

**Dr. Steven O. Dean**
Fusion Policy & History
*DOE / Fusion Power Associates · 2025–Present*

**Dr. Patrick H. Diamond**
Plasma Turbulence & Transport
*UC San Diego · 2025–Present*

**Dr. Jack J. Dongarra**
HPC & Numerical Algorithms
*Turing Award · 2025–Present*

**Dr. Nasr M. Ghoniem**
Chief Material Scientist
*UCLA · 2025–Present*

**Dr. Siegfried Glenzer**
Plasma Physics & Laser Fusion
*Stanford / SLAC · 2022–Present*

**Dr. David A. Hammer**
Pulsed-Power Fusion
*Cornell · 2025–Present*

**Dr. Donald A. Spong**
Plasma Theory & Confinement
*ORNL · 2025–Present*

**Dr. Curtis Smith**
Risk Assessment & Nuclear PRA
*MIT / Idaho National Lab · 2025–Present*

**RADM (Ret.) David Goggins**
Naval Engineering & Power-Plant Design
*U.S. Navy · 2023–2026*

**Dr. Konstantin Batygin**
Mathematician
*Caltech · 2022–2025*

**Dr. Ruben Fair**
Magnet Design / ITER Liaison
*PPPL / Jefferson Lab · 2022–2025*

**Dr. Paul S. Weiss**
Materials & Nanotechnology
*UCLA · 2022–2025*

## SCIENTIFIC AUDITORS

**Dr. Wilfred A. Cooper**
Plasma Equilibrium Theory
*EPFL / Swiss Plasma Center · 2025–Present*

**Dr. Ahmed Hassanein**
Plasma–Material Interactions
*Purdue / Argonne · 2025–Present*

**Dr. Patrick E. Hopkins**
Extreme Thermal Materials
*U. of Virginia · 2025–Present*

**Dr. Peter Hosemann**
Materials Joining & Structural Integrity
*UC Berkeley · 2025–Present*

**Dr. Travis W. Knight**
Advanced Nuclear Fuels & Systems
*U. of South Carolina · 2025–Present*

**Dr. Philippe Lebrun**
Cryogenics & Magnet Cooling
*CERN · 2025–Present*

**Dr. Nitendra Singh**
Nuclear Safety & Fuel Cycle
*ITER · 2025–Present*

**Dr. Guido Van Oost**
Magnetic Confinement & Fusion Systems
*Ghent University · 2025–Present*

**Dr. Gary S. Was**
Radiation Materials & Structural Integrity
*U. of Michigan · 2025–Present*

**Dr. Ray Sedwick**
Direct Energy Conversion
*U. of Maryland · 2025*

## OPERATIONS

**Michael Laughlin**
Chief Operating Officer
*2022–Present*

**Martin Owens**
Chief Strategy Officer
*LANL / GE Hitachi · 2022–Present*

**MG (Ret.) Paul Pardew**
Chief Contracting Officer
*Army Contracting Command · 2022–Present*

**David Beck**
Fusion Commercialization
*U.S. Space Force · 2024–Present*

**Sushma Bhatia**
Environmental & Legislative
*Google · 2022–Present*

**Michael De Frenza**
Technology Licensing
*2023–Present*

**MG (Ret.) Robin L. Fontes**
Cybersecurity & Defense
*Army Cyber Command · 2022–Present*

**Vijay Gehani**
Supply Chain & Components
*INOX India · 2024–Present*

**Jon Michel Greenwood**
IT & AI Infrastructure
*Live Nation · 2023–Present*

**Brian C. O'Neill**
National Security
*CIA / ODNI · 2022–Present*

**Gen. (Ret.) Gustave F. Perna**
DoD Liaison
*Operation Warp Speed · 2022–2023*

**Andrea Romero**
Marketing Lead
*2022–Present*

Legal counsel is retained; those roles are held on the internal roster and are not listed here.

SOURCES

# References


1 Y-K M Peng and D J Strickler, Features of spherical torus plasmas, *Nucl. Fusion* **26** 769 (1986).

2 J E Menard *et al*, Fusion nuclear science facilities and pilot plants based on the spherical tokamak, *Nucl. Fusion* **56** 106023 (2016). doi:10.1088/0029-5515/56/10/106023

3 B N Sorbom *et al*, ARC: a compact, high-field, fusion nuclear science facility and demonstration power plant with demountable magnets, *Fusion Eng. Des.* **100** 378 (2015). doi:10.1016/j.fusengdes.2015.07.008

4 M E Austin *et al*, Achievement of reactor-relevant performance in negative triangularity shape in the DIII-D tokamak, *Phys. Rev. Lett.* **122** 115001 (2019). doi:10.1103/PhysRevLett.122.115001

5 A Marinoni, O Sauter and S Coda, A brief history of negative triangularity tokamak plasmas, *Rev. Mod. Plasma Phys.* **5** 6 (2021). doi:10.1007/s41614-021-00054-0

6 O Sauter, C Angioni and Y R Lin-Liu, Neoclassical conductivity and bootstrap current fraction, *Phys. Plasmas* **6** 2834 (1999). doi:10.1063/1.873240

7 N J Fisch, Theory of current drive in plasmas, *Rev. Mod. Phys.* **59** 175 (1987).

8 F Troyon, R Gruber, H Saurenmann, S Semenzato and S Succi, MHD-limits to plasma confinement, *Plasma Phys. Control. Fusion* **26** 209 (1984).

9 J P Freidberg, *Ideal MHD*, Cambridge University Press (2014).

10 M E Sawan and M A Abdou, Physics and technology conditions for attaining tritium self-sufficiency for the DT fuel cycle, *Fusion Eng. Des.* **81** 1131 (2006).

11 M Abdou *et al*, Blanket/first wall challenges and required R&D on the pathway to DEMO, *Fusion Eng. Des.* **100** 2 (2015).

12 M J Norgett, M T Robinson and I M Torrens, A proposed method of calculating displacement dose rates, *Nucl. Eng. Des.* **33** 50 (1975).

13 G S Was, *Fundamentals of Radiation Materials Science: Metals and Alloys*, 2nd ed., Springer (2017).

14 V P Pastukhov, Collisional losses of electrons from an adiabatic trap in a plasma with a positive potential, *Nucl. Fusion* **14** 3 (1974).

15 R F Post, The magnetic mirror approach to fusion, *Nucl. Fusion* **27** 1579 (1987).

16 D E Baldwin and B G Logan, Improved tandem mirror fusion reactor, *Phys. Rev. Lett.* **43** 1318 (1979).

17 G I Dimov, V V Zakaidakov and M E Kishinevsky, Thermonuclear confinement with twin mirror systems, *Sov. J. Plasma Phys.* **2** 326 (1976).

18 T K Fowler and B G Logan, The tandem mirror reactor, *Comments Plasma Phys. Control. Fusion* **2** 167 (1977).

19 A A Bekhtenev, V I Volosov, V E Pal'chikov, M S Pekker and Yu N Yudin, Problems of a thermonuclear reactor with a rotating plasma, *Nucl. Fusion* **20** 579 (1980).

20 R F Ellis *et al*, Steady supersonically rotating plasmas in the Maryland Centrifugal Experiment, *Phys. Plasmas* **12** 055704 (2005). doi:10.1063/1.1896375

21 D Endrizzi *et al*, Physics basis for the Wisconsin HTS Axisymmetric Mirror (WHAM), *J. Plasma Phys.* **89** 975890501 (2023). doi:10.1017/S0022377823000806

22 P A Bagryansky *et al*, Threefold increase of the bulk electron temperature of plasma discharges in a magnetic mirror device, *Phys. Rev. Lett.* **114** 205001 (2015). doi:10.1103/PhysRevLett.114.205001

23 J Candy, E A Belli and R V Bravenec, A high-accuracy Eulerian gyrokinetic solver for collisional plasmas, *J. Comput. Phys.* **324** 73 (2016). doi:10.1016/j.jcp.2016.07.039

24 J Candy and R E Waltz, An Eulerian gyrokinetic-Maxwell solver, *J. Comput. Phys.* **186** 545 (2003). doi:10.1016/S0021-9991(03)00079-2

25 P K Romano, N E Horelik, B R Herman, A G Nelson, B Forget and K Smith, OpenMC: a state-of-the-art Monte Carlo code for

COLOPHON

# How this document was made

*The Kronos Fleet — Combined Editorial, 2026* is set in **Fraunces** (display), **Gelasio** (text), and **IBM Plex Mono** (data & equations), carried forward from the Kronos editorial design system.

The figures are rendered at 300 dpi from the deposited generator scripts; the document is composed as a single self-contained file with embedded fonts and imagery, paginated to US Letter, and rendered to PDF through a headless Chromium engine in matched light and dark editions.

Every headline quantity carries an evidence class; withdrawn and restated values are marked as such. Nothing herein is frozen beyond the founder-approved Tier-A set.

Explore it live — turn the interactive 3-D model, run the deposited solvers in the physics validator, and watch the companion film series.

LEGAL NOTICE

# Notice, status, and distribution

**Conceptual design & simulation study.** This document reports a conceptual design and simulation study. It is not a construction commitment, a safety-analysis report, a regulatory filing, or an offer of securities. Forward-looking statements — schedules, costs, market sizes, and performance — are estimates subject to the limitations set out in the Simulations part and may change.

**Numbers and their classes.** Quantities are reported with evidence classes and case labels; modelled, assumed, and requirement-class values are identified as such and are not to be quoted without their labels.

**Public edition.** This edition carries the physics and design only; all financial, funding, and defense-commercial content has been removed for public distribution. The scientific text corresponds to the arXiv and journal submissions.

THE 2026 KRONOS SERIES

# One programme, many papers

This editorial is one paper in the Kronos 2026 series — a real fusion company's complete, reproducible physics record for a spherical-tokamak breeder and its low-neutron D–$^{3}$He tandem-mirror burners. Every headline number is a frozen anchor in the Physics De-Risking Register.

Explore the whole programme: the De-Risking Register, the interactive 3-D model, and the physics validator.

KRONOS FUSION ENERGY

# *Red-Teaming the Frozen Design Point: Current-Drive and beta-Headroom Margins for a Spherical-Tokamak Breeder and Thermal-Barrier versus Centrifugal Plug Alternatives for the Mirror Burner*

A real fusion company building real machines. Explore the science, live.

Zenodo · doi:10.5281/zenodo.22645720

Read on kronosfusionenergy.com

The Physics De-Risking Register